Reverse Atom Transfer Radical Graft Polymerization of 4-Vinylpyridine onto Inorganic Oxide Surfaces

Gregory T. Lewis, Van Nguyen, Wen-Yi Shih, Yoram Cohen

Department of Chemical and Biomolecular Engineering, University of California, Los Angeles, California 90095-1592

Received 16 May 2008; accepted 27 December 2008
DOI 10.1002/app.29978
Published online 19 March 2009 in Wiley InterScience (www.interscience.wiley.com).

ABSTRACT: Thin poly(4-vinylpyridine) films terminally anchored onto nonporous inorganic oxide substrates were synthesized by aqueous phase reverse atom transfer radical graft polymerization (ATRGP). Surface initiators were immobilized on the inorganic substrate surface by chemically attaching glycidoxytrimethoxy silane onto the substrates followed by conversion of the glycidoxy silane into azobis silane by a reaction with 4,4′-azobis(4-cyanovaleric acid). Reverse ATRGP of 4-vinylpyridine onto the active surface azo sites was carried out in a 1-methyl-2-pyrrolidone/water solvent mixture using $CuCl_2$/2,2′-bipyridine as the catalyst-ligand complex with initial monomer concentration $[M]_0 = 2.32M$ at 90°C. Controlled radical polymerization was achieved at catalyst to initiator molar ratios of 2 : 1 and 3 : 1, with a catalyst to ligand molar ratio of 1 : 2. Controlled polymerization was indicated by a first-order rate of polymerization kinetics, with respect to monomer conversion at the surface and in solution, the linear increase of the P4VP graft yield with time, and a low polydispersity index (PDI < 1.40). The highest graft yield of 8 mg/m^2 was achieved at a 3 : 1 catalyst to initiator molar ratio which corresponded to a number-average molecular weight of 11,500 g/mol, surface density of 0.69 μmol/m^2, and a polydispersity index of 1.28. AFM surface analysis of the grafted polymer films, prepared by reverse ATRGP of 4VP, revealed a decrease in the RMS surface roughness ($R_{RMS} = 1.04$ nm) and feature size (feature diameter = 20–45 nm), relative to uncontrolled free radical graft polymerization ($R_{RMS} = 1.42$ nm; feature diameter = 60–145 nm), thereby providing an additional indication that a denser and controlled reaction was achieved via reverse ATRGP. © 2009 Wiley Periodicals, Inc. J Appl Polym Sci 113: 437–449, 2009

Key words: radical polymerization (ATRP); atomic force microscopy (AFM); films; nanolayers; radical polymerization

INTRODUCTION

Surface graft polymerization has evolved as a proven technology for modifying the surface properties of inorganic solid substrates so as to impart chemical selectivity of functional polymers in applications that include, for example, gas and liquid chromatography,[1–4] biocompatible materials,[5,6] colloidal stability,[7] and modified inorganic membranes.[8–12] Various methods of polymer surface modification have been proposed,[13,14] with free radical graft polymerization (FRGP) often being the method of choice given its simplicity for creating a dense polymer brush layer on a variety of substrate materials.[15–19] FRGP requires surface activation by a suitable initiator in the presence of a vinyl monomer for grafting. The properties of the graft polymerized chains, such as polymer graft yield (mg/m^2), number-average molecular weight (g/mol) and surface density (mol/m^2), can be controlled by adjusting synthesis parameters (e.g., temperature, reaction time, initial monomer concentration, initiator concentration and/or substrate loading).[18,19] However, despite efforts to control various aspects of the process, FRGP generally results in a broad grafted chain size distribution.[18,19]

In recent years, there has been a growing interest in atom transfer radical polymerization (ATRP)[20–33] and its application to graft polymerization in order to synthesize grafted polymers with narrow size distributions (i.e., polydispersity index in the range of 1.0–1.5).[34–42] Successful polymerization by both forward and reverse ATRP have been demonstrated for a number of monomers, including styrene, methyl methacrylate, acrylonitrile, acrylamide, acrylic acid, vinyl pyridine and some of their derivatives, with reported number-average degree of polymerization, $\overline{DP}$, and polydispersity index, PDI, in the range of 100–1,500 and 1.0–1.5, respectively.[20–33] Atom transfer radical graft polymerization (ATRGP), the adaptation of ATRP for surface graft polymerization, has achieved similar success in creating dense and relatively uniform polymer layers on gold,[43,44] silica,[45–47] silicon,[48–51] latex,[52,53] and polymeric substrates.[42,54,55] ATRGP, similar to ATRP, enables the control of radical graft polymerization by establishing a rapid

Correspondence to: Y. Cohen (yoram@ucla.edu).
Contract grant sponsors: California Department of Water Resources, U.S. Environmental Protection Agency.

equilibration between active surface chain radicals and those capped with a suitable control agent (e.g., halide).[20–33] Reversible capping of growing chains by the halide reduces the concentration of active ("live") chains, thereby lowering the rate of monomer addition and chain termination and allowing for enhanced control of the polymer chain size as well as polymer synthesis of a narrower molecular weight distribution, relative to "uncontrolled" FRGP. As halide exchange is reversible, graft polymerization by ATRP can be conducted in either the forward phase or the reverse phase. Forward ATRGP relies on a transition metal catalyst complex M_t^n/L (with metal M_t in the n oxidation state complexed with ligand L) that reversibly abstracts the halide from the organic-halide macroinitiator to form the higher oxidation state catalyst $X\text{-}M_t^{n+1}/L$ (with halide X) and an alkyl radical intiator.[21,23] Reverse ATRGP is initiated directly by an azo or peroxide radical initiator and either proceeds via monomer addition or by reversible deactivation by halide species donated from the catalyst complex $X\text{-}M_t^{n+1}/L$.[20,30] Reverse ATRGP is generally preferred for commercial application as the catalyst is less expensive, more oxidatively stable in air, and less sensitive to water than the catalyst used for forward ATRGP.[56] Also, the macroinitiator used in forward ATRGP has disadvantages, relative to conventional initiators, because of its potential toxicity, higher cost, and lower initiator efficiency.[56–58]

4-Vinylpyridine (4VP), which is the focus of this study, has been of particular interest because of its extensive applications in areas such as molecular imprinting polymers,[59,60] ion-exchange resins,[61–64] and microfiltration membranes.[65,66] Recently, it has been shown that free radical polymerization of 4VP, in a 50 vol % 1-methyl-2-pyrolidone/water mixture, can be controlled via reverse ATRP[67] where 2,2′-azobis(2,4-dimethylpentanitrile) and $CuCl_2$/dipyridyl were the initiator and catalyst-ligand complex, respectively. At a 1.6 : 1 molar ratio of $CuCl_2$ catalyst to azonitrile initiator, reverse ATRP of 4-vinylpyridine (initial concentration of 3.24*M*) was first-order with respect to monomer concentration and displayed linear chain growth with conversion, reaching a number-average molecular weight $\overline{M}_n$ = 26,000 g/mol and a polydispersity index PDI = 1.29.[67] Graft polymerization by forward ATRGP of 4VP has also been reported,[68–72] with successful controlled polymerization onto gold particles using a CuBr catalyst ($\overline{M}_n \sim$ 39,000 g/mol, PDI = 1.33).[73] However, reverse ATRGP of 4VP in an aqueous solvent mixture has yet to be demonstrated.

In this work, we demonstrate that controlled radical graft polymerization of 4VP onto silica in an aqueous solvent mixture can be accomplished by reverse ATRGP. Surface graft polymerization studies using nonporous silica particles served to identify the reaction conditions that enabled controlled graft polymerization. Local surface topography was assessed using tapping mode Atomic Force Microscopy on modified silicon wafers. Analysis of the polymerization data via standard reaction kinetic models served to evaluate the efficiency of surface grafting and the properties of the grafted polymer phase (e.g., average chain size, polydispersity index, surface chain density and chain spacing).

ANALYSIS OF POLYMERIZATION KINETICS

The reaction mechanism of reverse ATRGP involves initiation, propagation, and termination reactions, which also take place in FRGP (Table I). However, in reverse ATRGP, the number of active macroradicals (and thus the rate of termination of macroradicals) is significantly reduced because of reversible halide exchange. The kinetic mass balance equations for FRGP[18,19,74] and reverse ATRP[21–24] have been well described in the literature. As shown in Table I, in the reaction scheme involving surface-bound initiator SI_2, decomposition of the initiator produces a surface-immobilized initiator radical $SI^\bullet$ and a mobile free initiator radical $I^\bullet$ in solution, with initiator efficiencies of f_s and f_b, respectively. The initiator efficiency (i.e., grafting efficiency) in solution (f_s) is expected to be greater than the initiator efficiency at the surface (f_b), primarily due to monomer-initiator cage effects, which restrict diffusion of monomer to surface initiation sites, steric effects, and diffusion limitations near the solid surface due to the limited degrees of freedom of the surface anchored initiator species.[18] Subsequent to initiation, the initiator radicals $SI^\bullet$ and $I^\bullet$ can reversibly bind to Cl from the catalyst/ligand complex ($CuCl_2/L$), resulting in a chloride-capped initiator I-Cl. The initiator radicals $SI^\bullet$ and $I^\bullet$ can also activate a monomer molecule M to form monomer radicals on the surface ($SIM^\bullet$) or in the bulk ($IM^\bullet$), respectively, which, similar to FRGP, can grow (or propagate) and terminate.

Free radical graft polymerization

The kinetic expressions for both free radical graft polymerization (FRGP) and reverse ATRGP may be derived from the general expressions for the rate of surface and bulk polymerization, $R_{sp} \equiv k_p\,[SIM^\bullet][M]$ and $R_{bp} \equiv k_p\,[IM^\bullet\,][M]$, respectively (Table I). In the absence of reactions involving the catalyst-ligand complex, the classical expression for the rate of FRGP is obtained by invoking the standard pseudo-steady-state hypothesis (PSSH) and the long-chain hypothesis for radical species in solution,[18] assuming that monomer addition is the dominant path of chain growth. The resulting expression for the rate of free radical polymerization at the surface is

TABLE I
Reaction Scheme for Reverse ATRGP

Chain initiation

$$SI_2 \xrightarrow{k_d} SI^\bullet + I^\bullet \quad (1a)$$

$$SI^\bullet + M \xrightarrow{k_i} SIM_1^\bullet \quad (1b)$$

$$I^\bullet + M \xrightarrow{k_i} IM_1^\bullet \quad (1c)$$

Chain propagation

$$SIM_n^\bullet + M \xrightarrow{k_p} SIM_{n+1}^\bullet \quad (2a)$$

$$IM_n^\bullet + M \xrightarrow{k_p} IM_{n+1}^\bullet \quad (2b)$$

$$SIM_n^\bullet + CuCl_2/L \underset{k_{act}}{\overset{k_{deact}}{\rightleftharpoons}} SIM_n - Cl + CuCl/L \quad (3a)$$

$$IM_n^\bullet + CuCl_2/L \underset{k_{act}}{\overset{k_{deact}}{\rightleftharpoons}} IM_n - Cl + CuCl/L \quad (3b)$$

Chain transfer

$$SIM_n^\bullet + X \xrightarrow{k_{trX}} SIM_n + X^\bullet \quad (4a)$$

$$IM_n^\bullet + X \xrightarrow{k_{trX}} IM_n + X^\bullet \quad (4b)$$

Chain termination

$$SIM_m^\bullet + SIM_n^\bullet \xrightarrow{k_{tc}} SIM_m + SIM_n \quad (5a)$$

$$SIM_m^\bullet + IM_n^\bullet \xrightarrow{k_{tc}} SIM_m + IM_n \quad (5b)$$

$$IM_m^\bullet + IM_n^\bullet \xrightarrow{k_{tc}} IM_m + IM_n \quad (5c)$$

$$SIM_m^\bullet + SIM_n^\bullet \xrightarrow{k_{td}} SIM_m - SIM_n \quad (5d)$$

$$SIM_m^\bullet + IM_n^\bullet \xrightarrow{k_{td}} SIM_m - IM_n \quad (5e)$$

$$IM_m^\bullet + IM_n^\bullet \xrightarrow{k_{td}} IM_m - IM_n \quad (5f)$$

$$R_{sp} \equiv k_p[SIM^\bullet][M] = k_p\left(\frac{f_s}{f_b}\right)\left[\frac{f_b k_d}{2k_t}\right]^{1/2}[SI_2]^{1/2}[M] \quad (6a)$$

with a similar expression for the rate of monomer consumption in the bulk solution

$$R_{bp} \equiv k_p[IM^\bullet][M] = k_p\left[\frac{f_b k_d}{2k_t}\right]^{1/2}[SI_2]^{1/2}[M] \quad (6b)$$

where k_p, k_d, and k_t are the rate coefficients for monomer propagation, initiator decomposition, and polymer chain termination (i.e., combination and disproportionation, $k_t = k_{tc} + k_{td}$), respectively. It is assumed that the propagation rate coefficient for R_{sp} [eq. (6a)] and R_{bp} [eq. (6b)] are of the same magnitude for both surface chains and chains formed in solution.[18] The total rate of monomer consumption (or total rate of polymerization), which is the sum of the above two polymerization rates [eqs. 6(a,b)], is then

$$R_M \equiv R_{sp} + R_{bp} = k_p\left(\frac{f_s}{f_b} + 1\right)\left[\frac{f_b k_d}{2k_t}\right]^{1/2}[SI_2]^{1/2}[M] \quad (7)$$

and the temporal evolution of monomer concentration as a result of both surface and bulk polymerization can be obtained by integrating eq. (7) to obtain the following expression

$$\ln\left(\frac{[M]_0}{[M]}\right) = -\ln(1-\varphi) = 2\frac{k_p}{k_d}\left(\frac{f_s}{f_b} + 1\right)\left[\frac{f_b k_d}{2k_t}\right]^{1/2}[SI_2]_0^{1/2}\left(1 - e^{-fk_d t/2}\right) \quad (8)$$

where monomer conversion is defined as $\varphi = ([M]_0 - [M])/[M]_0)$, the initiator decomposition (i.e., $[SI_2] = [SI_2]_0 e^{-fk_d t}$) follows first-order kinetics and $[SI_2]_0$ and $[M]_0$ are the initial concentrations of initiator and monomer in solution, respectively.

Reverse atom transfer radical graft polymerization

The rapid equilibrium approximation is appropriate for the reversible halide exchange that takes place in reverse atom transfer radical graft polymerization (ATRGP).[22,23] Accordingly, the following expressions for the concentrations of surface-bound initiated chains and solution initiated chains have been proposed[28,40]:

$$k_{deact}[SIM^\bullet]^*[CuCl_2/L]^* = k_{act}[SIM - Cl]^*[CuCl/L]^* \quad (9a)$$

$$k_{deact}[IM^\bullet]^*[CuCl_2/L]^* = k_{act}[IM - Cl]^*[CuCl/L]^* \quad (9b)$$

where k_{deact} and k_{act} are the deactivation and activation rate constants for the controlled polymerization reaction; the superscript * indicates steady-state concentrations; and $[SIM^\bullet]^*$ and $[IM^\bullet]^*$ which can be expressed as[28,40]

$$[SIM^\bullet]^* = \frac{k_{act}}{k_{deact}}\frac{[SIM - Cl]^*[CuCl/L]^*}{[CuCl_2/L]^*} = K\frac{[SIM - Cl]^*[CuCl/L]^*}{[CuCl_2/L]^*} \quad (10a)$$

$$[IM^\bullet]^* = \frac{k_{act}}{k_{deact}}\frac{[IM - Cl]^*[CuCl/L]^*}{[CuCl_2/L]^*} = K\frac{[IM - Cl]^*[CuCl/L]^*}{[CuCl_2/L]^*} \quad (10b)$$

The rates of polymerization (or monomer consumption) by reverse ATRP for surface-graft polymerization and monomer consumption in solution is obtained by the combination of eq. 6(a,b) with eqs. 10(a,b) to give the following expressions:

$$R_{sp} \equiv k_p[SIM^\bullet]^*[M] = k_pK\frac{[SIM-Cl]^*[CuCl]^*}{[CuCl_2]^*}[M] = K_{app,s}[M] \quad (11a)$$

$$R_{bp} \equiv k_p[IM^\bullet]^*[M] = k_pK\frac{[IM-Cl]^*[CuCl]^*}{[CuCl_2]^*}[M] = K_{app,b}[M] \quad (11b)$$

where $K_{app,s} \equiv k_p$ K[SIM − Cl]*[CuCl]*/[$CuCl_2$]* is the apparent kinetic rate coefficient for surface polymerization and $K_{app,b} \equiv k_p$ K[IM − Cl]*[CuCl]*/[$CuCl_2$]* is the corresponding apparent kinetic rate coefficient for bulk solution polymerization. The overall rate of polymerization (or monomer consumption) by surface and bulk polymerization is given as the sum of eqs. 11(a,b):

$$R_M \equiv R_{sp} + R_{bp} = (K_{app,s} + K_{app,b})[M] \quad (12)$$

with the temporal change of monomer concentration (and thus monomer conversion), due to surface and bulk polymerization obtained from the integration of eq. (12):

$$\ln\left(\frac{[M]_0}{[M]}\right) = -\ln(1-X) = \left(K_{app,s} + K_{app,b}\right)t \quad (13)$$

The growth of the grafted polymer layer, as evaluated based on the experimental surface polymer graft yield (G_p, mg of surface grafted monomer/m^2 silica surface), is the combination of the rate of monomer addition to surface chains (R_{sp}) and the rate of grafting of bulk chains formed in solution onto the surface (R_{st}), as expressed by[18]

$$\frac{(S_L)(\varepsilon)}{M_m}\frac{dG_p}{dt} = R_{sp} + R_{st}\overline{DP_b} = k_p[SIM_n^\bullet][M] + \overline{DP_b}\xi[SIM_n^\bullet][IM_n^\bullet] \quad (14)$$

in which S_L is the initial amount of substrate loading (g of silica/L of solution), ε is the specific surface area of the substrate (m^2 of silica surface/g of silica), M_m is the molar mass of the monomer unit, $\overline{DP}_b$ is the number-average degree of polymerization of the chains formed in the bulk solution, and ξ is the probability that a chain will terminate by a combination reaction rather than by disproportionation. For FRGP, it is apparent from eq. (14) that the temporal evolution of G_p would be nonlinear with respect to time. In contrast, for reverse ATRGP, the rate of termination is negligible, relative to the rate of propagation, because of the small fraction of uncapped active radical chains that are present in solution. Therefore, for reverse ATRGP, when [$SIM_n^\bullet$] and [$IM_n^\bullet$] are low (given the low concentration of surface grafted initiator and for low substrate loading), the second term on the right hand side of eq. (14) should be negligible and, as a result, the graft yield G_p would be expected to increase linearly with time. It is also noted that the fraction of bulk monomer which has been consumed by surface graft polymerization or contained in polymer chains that are grafted to the surface from solution, f_s^m, can be evaluated from the measured surface polymer graft yield as

$$f_s^m = \left([M]_0 - \int_0^t \frac{(S_L)(\varepsilon)}{M_m}\frac{dG_p}{dt}dt\right)\Big/[M]_0 \quad (15)$$

Under reverse ATRGP,ln ($1/f_s^m$) would increase linearly with time, consistent with the expectation of the first order dependence of R_{sp} [eq. (11a)] on solution monomer concentration and the dependence of dG_p/dt on R_{sp} [eq. (14)].

EXPERIMENTAL SECTION

Materials

Nonporous silica particles (Novacite L207-A), obtained from Malvern Minerals (Hot Springs, AK), were 5 μm in size with a specific surface area, measured by BET nitrogen adsorption,[18,19] of 2.2 m^2/g. Deionized (DI) water was produced using a Millipore (Bedford, MA) Milli-Q filtration system. 3-Glycidoxypropyltrimethoxysilane (98%) and anhydrous toluene (99.8%) used in the silylation reaction, 4,4′-azobis(4-cyanovaleric acid) (75+%), ACS-grade dimethylsulfoxide (99.9%) solvent for the conversion of glycidoxy silane into azo silane, $CuCl_2$ (99+%) that served as a catalyst in the reverse ATRGP reactions, 2,2′-bipyridine (99+%) used as the ligand in the reverse ATRGP reactions, and HPLC-grade acetonitrile (99.93+%) used in size exclusion chromatography (SEC) were obtained from Sigma-Aldrich (Milwaukee, WI). 2-Picoline (98+%) used as the catalyst for the conversion of glycidoxy silane into azo silane, 1-methyl-2-pyrrolidone (99%+) used as a solvent component for the reverse ATRGP reactions, 4-vinylpyridine (96%+) monomer, and sodium nitrate (99%+) used in the SEC mobile phase were obtained from Lancaster Synthesis (Windham, NH). Narrow molecular-weight standards of sodium polystyrene sulfonate (PDI = 1.08-1.10), employed in calibrations of the SEC column, were purchased from Polysciences (Warrington, PA).

Grafting of azo Initiators onto silica particles

Graft polymerization reactions were performed using nonporous silica particles. Prior to radical

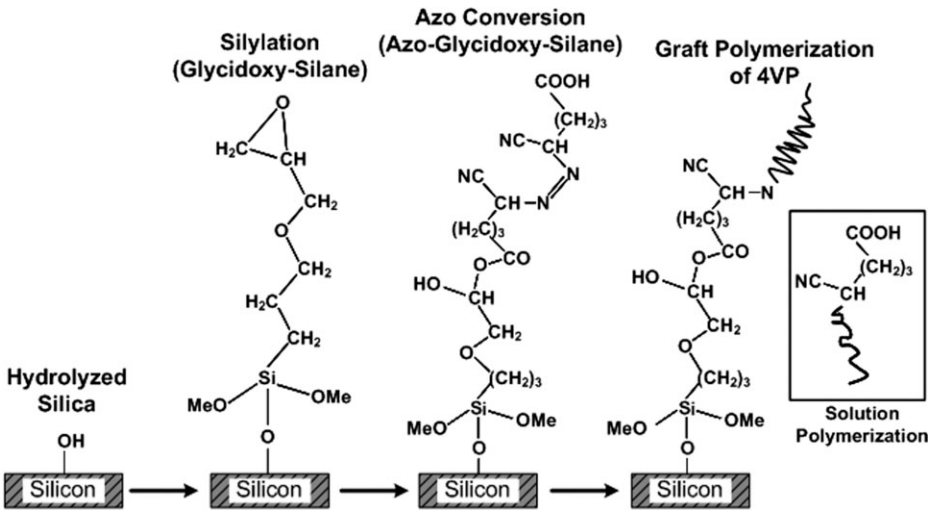

Figure 1 Reaction scheme for graft polymerization of 4-vinylpyridine onto silica.

graft polymerization of 4VP, the silica particles were chemically modified with the azo initiator using a two-step process, following the method of Tsubokawa et al.[15,16] In the first step, the particles, which had been washed with DI water and dried/equilibrated at room conditions, were silylated with 5 vol% of 3-glycidoxypropyltrimethoxysilane in anhydrous toluene ($\sim$ 0.1 g silica/ml toluene) in a well-capped glass jar for 24 h at room temperature [Fig. 1]. A typical reaction involved 20 g of silica particles and 200 mL of the 3-glycidoxypropyltrimethoxysilane/toluene mixture. Subsequently, the particles were washed with excess toluene to remove any unreacted silane and were vacuum dried at 100°C. In the second step, surface glycidoxy groups were converted into azo groups through a reaction with 4,4′-azobis(4-cyanovaleric acid) [Fig. 1]. A typical reaction was conducted at 50°C in 50 mL of dimethylsulfoxide (DMSO), 0.5 g of 4,4′-azobis(4-cyanovaleric acid) and 0.5 ml of 2-picoline catalyst. The glycidoxy-grafted particles were then added to the mixture and the reaction was allowed to proceed. At the termination of the reaction period ($\sim$ 24 h), the reaction mixture was filtered using a Teflon membrane (1 μm pore size), washed extensively with ethanol and dried at room temperature for 12 h.

Graft polymerization of P4VP onto silica particles

The effect of $CuCl_2$ catalyst to initiator molar ratio for reverse ATRGP of 4VP onto azo-grafted particles was evaluated at a reaction temperature of 90°C and an initial monomer concentration $[M]_0 = 2.32M$ in a 50 vol % 1-methyl-2-pyrrolidone/water solvent mixture. The aforementioned reaction condition was previously shown to enable controlled reverse ATRP homopolymerization in solution.[67] At these conditions, reasonable conversion (up to about 60%) was achieved over a 24 h reaction period without excessive increase in the viscosity of the solution, thereby enabling good mixing to be maintained. Graft polymerization reactions were conducted at four different $CuCl_2$ to initiator molar ratios of 0 : 1, 1 : 1, 2 : 1, and 3 : 1 and at a 2,2′-bipyridine ligand to $CuCl_2$ catalyst molar ratio of 2 : 1. The $CuCl_2$ and 2,2′-bipyridine ligand were added to each reaction tube, followed by the additions of 7.5 mL of the 50 vol % 1-methyl-2-pyrrolidone/water mixture and 2.5 mL of 4VP ($[M]_0 = 2.32M$). Subsequently, the liquid mixture in the septum-capped tubes was degassed by bubbling nitrogen (via feed and vent tubes inserted through the septum). Graft polymerization was initiated by transferring the liquid mixture into a Pyrex glass tube (previously nitrogen purged) containing the desired amount of the initiator-grafted particles ($\sim$ 5 g). At various intervals, small aliquots of the reaction slurry were withdrawn and centrifuged ($\sim$ 5,000 rpm for 5 minutes to sediment the silica particles). The supernatant liquid solution was then dosed with 5 mL of $0.05M$ $NaNO_3$ and 50 vol % HPLC grade acetonitrile in DI water for subsequent SEC analysis. SEC analysis was used to determine the total monomer conversion, number-average degree of polymerization ($\overline{DP}_b$), and polydispersity index (PDI). The graft polymerized silica particles were dispersed in 5 mL of denatured ethanol and the mixture was centrifuged for 10 min and then decanted; this step was repeated five times. Subsequently, the particles were vacuum-dried at 50°C and stored in a sealed vial for FTIR and TGA surface analyzes.

Graft polymerization of P4VP onto silicon oxide wafers

Silicon wafers were used as test surfaces to enable Atomic Force Microscopy (AFM) analysis of the

surface topography of the glycidoxy-grafted, azo-grafted and P4VP graft polymerized surfaces. Unmodified samples (2.5 × 2.5 cm^2) of prime-grade silicon wafers (Wafernet, San Jose, CA) were first soaked in acetone for 1 h and immersed for 3 h in a mixture of 70 : 30 sulfuric acid to hydrogen peroxide at 25°C (caution: this solution reacts violently with many organic materials and should be handled with extreme care). The wafer samples were then rinsed extensively with DI water and vacuum dried at 110°C. Surface modification of the cleaned wafer samples with 3-glycidoxypropyltrimethoxysilane was performed in a solution of 5 vol % 3-glycidoxypropyltrimethoxysilane in anhydrous toluene (~ 40 mL solution in a 100 mL reaction vessel). Glycidoxy-grafted surfaces were then reacted with 4,4′-azobis(4-cyanovaleric acid) in a mixture that also contained 2-picoline in DMSO. The initiator-grafted wafers were then graft polymerized with 4VP following the same procedure used for the silica particles. At the termination of the graft polymerization step, the wafer samples were washed extensively with ethanol, vacuum-dried at 50°C and stored in sealed containers for AFM analyzes.

Analysis

Surface functional groups for the modified silica particles were identified by Diffuse Reflectance Infrared Fourier Transform (DRIFT) spectroscopy using a BioRad FTS-40 FTIR equipped with a BioRad diffuse reflectance accessory (BioRad Digilab Division, Cambridge, MA). DRIFT IR spectra for glycidoxy-grafted, azo-grafted, and P4VP-grafted surfaces were obtained and further processed by subtraction of the DRIFT spectra from the unmodified native silica particles. All spectra are reported in terms of Kubelka-Munk absorbance units.[75]

The graft yields (mg/m^2) for the various surface modifiers (i.e., glycidoxy, azo and P4VP) grafted onto the particles were determined by thermogravimetric analysis[18,19] using a TGS-2 Perkin-Elmer thermogravimetric analyzer (Norwalk, CT). Analysis were carried out with the particle samples (~ 10 mg) first held at 110°C for 10 min (to remove adsorbed water) and then heated at a rate of 30°C/min up to 700°C, with the sample held at the final temperature for 10 min. Monomer concentration, number-average degree of polymerization and the polydispersity index were determined by size exclusion chromatography (SEC). The SEC system consisted of dual Waters 590 pumps (Milipore, Milford, MA), a Rheodyne 750 injection valve (Rheodyne, Rohnert Park, CA), a Tosohaas G6000PW column (Tosohaas, Montgomeryville, PA) and a Bio-Rad 1750 refractive index detector (Bio-Rad Laboratories, Richmond, CA). SEC measurements were carried out with a mobile phase consisting of 0.05*M* $NaNO_3$ with 50 vol % HPLC grade acetonitrile in DI water at a flow rate of 1.0 mL/min. The mobile phase selected was based on recommendations by the SEC column manufacturer (Tosohaas, Montgomeryville, PA) for P4VP analysis with a Tosohaas G6000PW column (packed with crosslinked hydroxylated polyether SEC resin beads). SEC chromatograms were recorded using a PSS 246 data acquisition unit and analyzed using the PSS WinGPC 6 software (Polymer Standards Service GmbH, Silver Spring, MD) for the number-average degree of polymerization and polydispersity index of poly(4-vinylpyridine) chains formed in solution. The column was calibrated using narrow molecular weight standards of sodium polystyrene sulfonate.

Monomer concentration was determined by utilizing 1-methyl-2-pyrrolidone (MP) as an internal standard given that this component was not consumed in the polymerization reaction. Accordingly, the ratio of monomer concentration to its initial value was obtained from:

$$\frac{[\mathrm{M}]_{t>0}}{[\mathrm{M}]_{t=0}} = \frac{([A_{4\mathrm{VP}}]/[A_{\mathrm{MP}}])_{t>0}}{([A_{4\mathrm{VP}}]/[A_{\mathrm{MP}}])_{t=0}} \tag{16}$$

where A_{4VP} and A_{MP} denote the areas under the 4VP peak and the MP peak, respectively, and t is the reaction time.

Surface topography of the native and modified wafers were obtained via AFM imaging (MultiMode III, Veeco Instruments, Santa Barbara, CA) operated in the tapping mode. AFM images were obtained for 0.5 × 0.5 μm^2 areas at a scan rate of 1 Hz. To exclude image artifacts, trace and retrace scans were performed from left to right and right to left, respectively. Surface imaging at 90° rotation of the scan direction was also carried out for each sample to detect possible directionally dependent features or artifacts and to optimize scan parameters.[19] The surface topography was analyzed to obtain the feature height histograms, surface material volume and relative change in feature elevations upon modification. The surface topography was also characterized in terms of the root mean squared (RMS) surface roughness, R_{RMS}, and skewness, S_{skew}, of the height histograms:

$$R_{\mathrm{RMS}} = \sqrt{\frac{\sum(Z_i - Z_{\mathrm{avg}})^2}{N}} \tag{17}$$

$$S_{\mathrm{skew}} = \frac{\sum(Z_i - Z_{\mathrm{avg}})^3}{(N-1)\cdot\sigma^3} \tag{18}$$

where N is the sample sizes in the x and y directions (on the substrate), Z_{avg} is the mean height, and σ is the standard deviation.

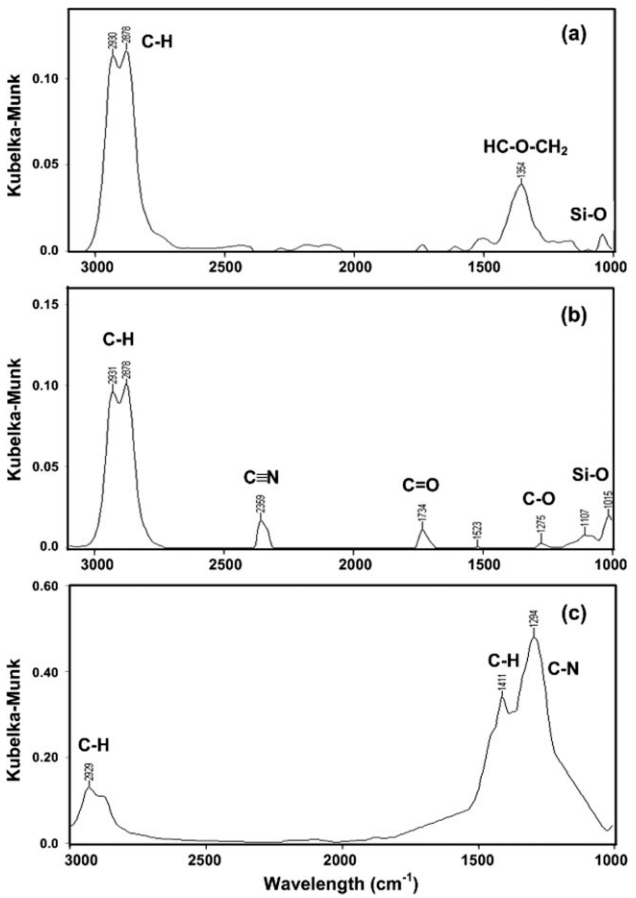

Figure 2 Diffuse reflectance IR spectra of (a) glycidoxy-grafted silica, (b) azo-grafted silica and (c) P4VP-grafted silica by reverse ATRGP.

RESULTS AND DISCUSSION

Chemical grafting of glycidoxy and azo functional groups

Azo initiators were chemically grafted onto silica using a two-step process [Fig. 1] involving: (1) surface silylation with 3-glycidoxypropyltrimethoxysilane, and (2) subsequent conversion of glycidoxy-silylated functional groups to azo silane using 4,4′-azobis(4-cyanovaleric acid). Chemical grafting of glycidoxy, azo, and P4VP onto silica was confirmed by DRIFT spectra [Fig. 2]. The IR spectrum of glycidoxy-grafted silica particles [Fig. 2(a)] revealed C—H bond stretching (near 3000 cm^{-1}), as well as bond stretching associated with the glycidoxy ring (at 1354 cm^{-1}). Modification of glycidoxy-grafted silica to form azo-grafted particles [Fig. 2(b)] resulted in an IR spectrum with peaks corresponding to bond stretching of C—H (near 3000 cm^{-1}), C≡N (at 2359 cm^{-1}), C=O (at 1734 cm^{-1}) and C—O (at 1275 cm^{-1}). IR spectrum of P4VP-grafted silica particles [Fig. 2(c)] revealed broader peaks associated with C—H bonds in the polymer backbone (near 3000 cm^{-1}), C—H bonds present in the pyridine ring (at 1411 cm^{-1}), and bond stretching of C—N (at 1294 cm^{-1}). The graft mass density of glycidoxy silylated onto the silica particles was 7.6 mg/m^2 ~ (32.3 μmol/m^2 or 19.4 molecules/nm^2) and the graft mass density of the azo was 3.5 mg/m^2 (12.3 μmol/m^2 or 7.4 molecules/nm^2). The conversion efficiency of glycidoxy silane to azo silane was about 38% ± 4%. Thus, the surface number density of azo groups grafted on glycidoxy-modified silica was equivalent to about 7.4 surface initiators/nm^2. The native silanol (or hydroxyl groups) on hydroxylated silica is ~ 7.6 μmol/m^2 (4.6 molecules/nm^2).[76] Therefore, 1.6 azo initiator groups were grafted for each native surface silanol and were at a higher surface azo grafting density relative to earlier studies.[16,17,77]

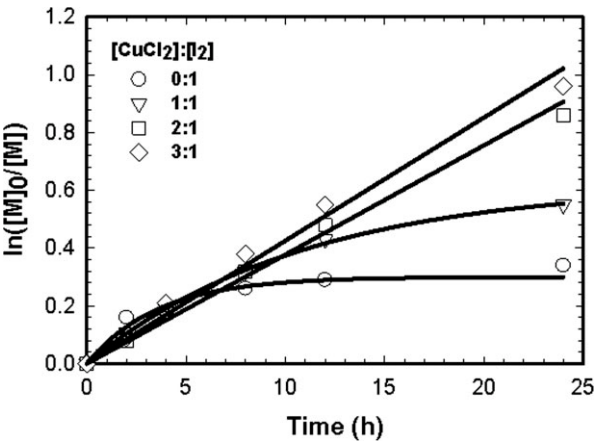

Figure 3 Data of (a) total conversion for reverse ATRGP of 4VP onto silica. $[M]_0$ = 2.32 *M*, $[I_2]_0$ = 13.6 m*M*, and *T* = 90°C. Catalyst concentrations are given in the legends.

Total and surface polymerization by FRGP and reverse ATRGP

The impact of catalyst to surface initiator ratio on the control of homopolymerization in solution [Fig. 3] and

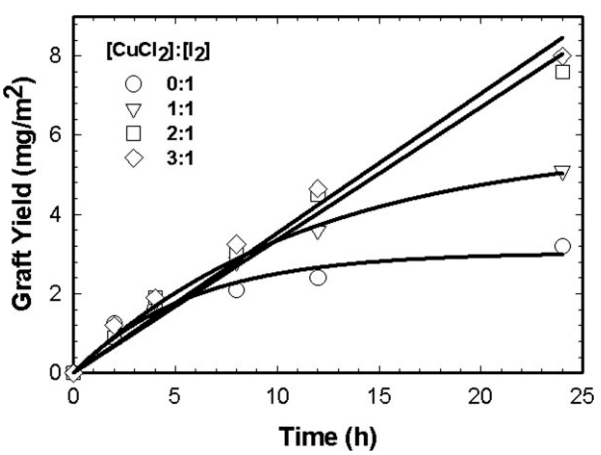

Figure 4 Polymer graft yield for reverse ATRGP of 4-vinylpyridine onto silicon as a function of reaction time. $[M]_0$ = 2.32*M*, $[I_2]_0$ = 13.6 m*M*, and *T* = 90°C. Catalyst concentrations are given in the legend.

surface graft polymerization [Fig. 4] indicated that reverse ATRGP of 4VP may be achieved for a 2 : 1 catalyst to surface initiator ratio. Graft polymerization of 4VP onto azo-grafted particles was carried out at 90°C, an initial monomer concentration $[M]_0 = 2.32M$, and an initial surface initiator density of 3.5 mg/m^2. Control of the graft polymerization reaction was assessed by verifying that the rate of monomer consumption was linear with respect to monomer concentration, the number-average degree of polymerization increased linearly with monomer conversion, and the polydispersity index was independent of conversion and was significantly below the polydispersity index expected for FRGP. Homopolymerization and surface graft polymerization of 4VP was initiated by the decomposition of the surface grafted azo, creating initiators at the surface and in the bulk solution. As a result, homopolymerization in solution occurred simultaneously with surface graft polymerization. The addition of the $CuCl_2$/2,2′-bipyridine catalyst complex to the reaction mixture resulted in control of both solution and surface graft polymerization reactions. The change in monomer concentration in the reaction mixture, depicted in terms of $\ln([M]_0/[M])$ or the equivalent $-\ln(1-\varphi)$ (where φ denotes monomer conversion), approached first-order kinetics with respect to monomer concentration as the catalyst to initiator ratio was increased above unity [Fig. 3]. As implied by eq. (13), a linear evolution of $\ln([M]_0/[M])$ with time attained for a 2 : 1 catalyst to surface initiator ratio suggests that controlled polymerization was achieved. On the other hand, for FRGP in the absence of catalyst (i.e., 0 : 1 catalyst to initiator ratio), the rate of monomer consumption deviated from first-order kinetics over the course of the reaction period [Fig. 3]. This behavior may be attributed to uncontrolled chain transfer [eqs. 4(a,b), where X denotes a chain transfer agent, which could also be the monomer itself], and chain termination reactions [eqs. 5(a–f)] which are characteristic of FRGP reactions. For the reverse ATRGP system, a total monomer conversion in solution of 43%, 58%, 62% was achieved for catalyst to initiator ratios of 1 : 1, 2 : 1, and 3 : 1, respectively, over the 24 h reaction period. In contrast, FRGP of 4VP (i.e., 0 : 1 catalyst to initiator ratio) resulted in a significantly lower total monomer concentration of about 29% for the 24 h reaction period. The lower conversion achieved with FRGP, relative to reverse ATRGP, was not surprising, given that reverse ATRGP reduces termination reactions and favors the progressive addition of monomer to chains both in solution and those tethered to the surface [eq. 3(a,b)].

Control of surface graft polymerization was demonstrated in the linear increase in polymer graft yield with reaction time [eq. (14)] for the catalyst to initiator ratios of 2 : 1 and 3 : 1, as shown in Figure 4. As the catalyst to surface initiator ratio was increased from 1 : 1 to 3 : 1, the polymer graft yield after 24 h increased by 60% from 5.1 to 8.2 mg/m^2. The linear increase in graft yield is consistent with eq. (14) when the contribution from polymer grafting, chain transfer and termination reactions are negligible. In contrast, for FRGP reaction conditions whereby surface graft polymerization occurs in the absence of the copper catalyst complex, the polymer graft yield after 24 h was only 2.94 mg/m^2. The decrease in polymer graft yield was due to the early termination reactions associated with chain transfer, surface-surface chain combination [eqs. 5(a,d)], and solution-surface chain combination [eqs. 5(b,e)] which may occur in free radical graft polymerization. Analogous to the methodology used to control homopolymerization reactions in solution, the graft yield may be increased by using the copper catalyst complex to reversible cap the growing polymer chains at the surface. The increase of the polymer graft yield with the molar ratio of catalyst to surface initiator [Fig. 4] suggests that the grafted chains were more efficiently and effectively protected from early termination, and thus a linear increase of polymer grafted yield was obtained.

The linear increase in the number-averaged degree of polymerization [$\overline{DP}$, Fig. 5(a)] with monomer concentration and the low polydispersity index [PDI, Table II, Fig. 5(b)] of 1.3 and 1.28 after a 24 h reaction period at catalyst to initiator ratios of 2 : 1 and 3 : 1, respectively, confirmed that controlled reverse ATRGP of P4VP was achieved. For controlled reverse ATRGP of 4VP, the P4VP chain size increased linearly with conversion [Fig. 5(a)] and reached a $\overline{DP}$ of 115 and 110 for a reaction time of 24 h at catalyst to initiator ratios of 2 : 1 and 3 : 1, respectively. The dependence of $\overline{DP}$ on monomer concentration [eq. (14)], for solution formed chains, was expected to be linear, as indeed was the case for successful reverse ATRGP [Fig. 5(a)]. Also, the PDI was independent of monomer conversion [Fig. 5(b)] and, for a catalyst to initiator ratio of 2 : 1, approached a PDI of 1.3, which is demonstrative of a reasonably controlled polymerization reaction. In contrast, for FRGP reaction conditions (i.e., catalyst to surface initiator ratio of 0 : 1), little or no control of chain growth was observed, as indicated by the increase in the PDI (PDI = 1.72). It is noted that for FRGP, the $\overline{DP}$ was significantly higher ($\overline{DP} = 288$) than for reverse ATRGP (Table II). The higher $\overline{DP}$ for FRGP is consistent with uncontrolled radical polymerization, where higher molecular weight macromolecular chains are formed in relatively short time periods at low monomer conversion.[18,74] It is noted that, although direct determination of the molecular weight of surface-grafted polymer chains (e.g., SEC) was not feasible, demonstration of polymer control

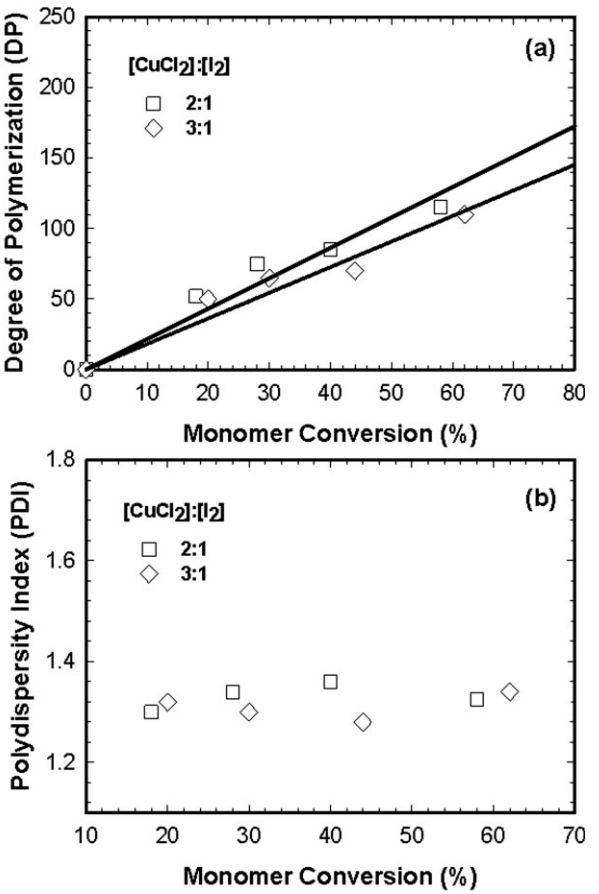

Figure 5 Controlled reverse ATRGP of 4-vinylpyridine: (a) number-average degree of polymerization ($\overline{DP}$) and (b) polydispersity index (PDI). $[M]_0 = 2.32M$, $[I_2]_0 = 13.6$ mM, and $T = 90°C$. Catalyst concentrations are given in the legends.

for solution polymerization and the linear growth of the grafted polymer are convincing indicators that a reasonable level of reverse ATRGP control was attained over the course of the reaction.

The calculated polymer graft densities exhibited a sixfold increase from 0.11 μmol/m^2 to 0.69 μmol/m^2 after a reaction period of 24 h as the catalyst to initiator ratio was increased from 0 : 1 to 3 : 1, respectively, demonstrating that chain protection from early termination by reverse ATRGP enabled higher grafting efficiency. The average molar density of grafted chains (GD, mmol/m^2) was estimated from the following relation:[18]

$$\mathrm{GD} = \frac{\mathrm{GY}}{\overline{DP} \cdot \mathrm{M}_m} \tag{19}$$

where GY is the graft yield (mg/m^2), $\overline{DP}$ is approximated by the degrees of polymerization of the polymer formed in solution (attained by SEC), and M_m is the monomer (4VP) molar mass. The average chain spacing, D, corresponding to the previous surface polymer chain density, was estimated based on the approximation of evenly spaced square grids of anchoring sites on a flat surface:[18]

$$D = \frac{1}{\sqrt{\mathrm{GD} \cdot N_A}} \tag{20}$$

where N_A denotes the Avogadro number. For the present range of reaction conditions (Table II), average chain spacing ranged from 39.6 Å to 15.5 Å for the initiator to catalyst ratio range of 0 : 1 to 3 : 1, respectively. The average chain spacing decreased sharply with increased catalyst concentration, consistent with the observed increase in the polymer graft density. The aforementioned trend suggests that a higher efficiency of monomer addition is obtained with reverse ATRGP relative to FRGP. The graft fraction (GF), which is defined as the ratio of grafted polymer monomer conversion (φ_{surf}) to total monomer conversion (φ_{tot}), similarly increased with catalyst to surface initiator ratios for the controlled reverse ATRGP reaction. The grafted polymer monomer conversion (φ_{surf}) can be determined based on the experimental polymer graft yield

$$\varphi_{surf} = \left(\frac{\mathrm{GY} \cdot S_A \cdot m_o}{\mathrm{M}_m \cdot [\mathrm{M}]_0}\right) \tag{21}$$

where $S_A = 2.2$ m^2/g is the specific area of the particles, and m_o is the particle mass concentration in the reaction mixture. The total monomer conversion to polymer (φ_{tot}) can be evaluated from $\varphi_{tot} = 1 - [M]/[M]_0$. For the case in which the ratio of initiator efficiency for SI_2 azo initiators at the surface and in solution was unity ($f_s = f_b$), and when chain transfer to monomer or solvent is negligible (in the case of controlled reverse ATRGP), the ratio of the rates of polymerization at the surface [R_{sp}, eq. (6a)] and in solution [R_{bp}, eq. (6b)] would likewise be unity and the maximum graft fraction would be 50%. However, for controlled reverse ATRGP, capped polymer chains in solution have a lower probability of

TABLE II
Number-Average Degree of Polymerization ($\overline{DP}$) and Poiydispersity Index (PDI) for FRGP and Controlled Reverse ATRGP for a Range of Catalyst to Initiator Molar Ratios at $[M]_0 = 2.32$ M, $[I_2]_0 = 13.6$ mM, and $T = 90°C$

	$[CuCl_2]$: $[I_2]_0$	$\overline{DP}$[a]	PDI[b]	Average chain spacing, D (Å)
FRGP	0 : 1	288	1.88	39.6
	1 : 1	270	1.72	30.4
Reverse ATRGP	2 : 1	115	1.30	16.2
	3 : 1	110	1.28	15.5

[a] Represents the maximum $\overline{DP}$ achieved under the present reaction conditions.
[b] Represents the maximum PDI achieved under the present reaction conditions.

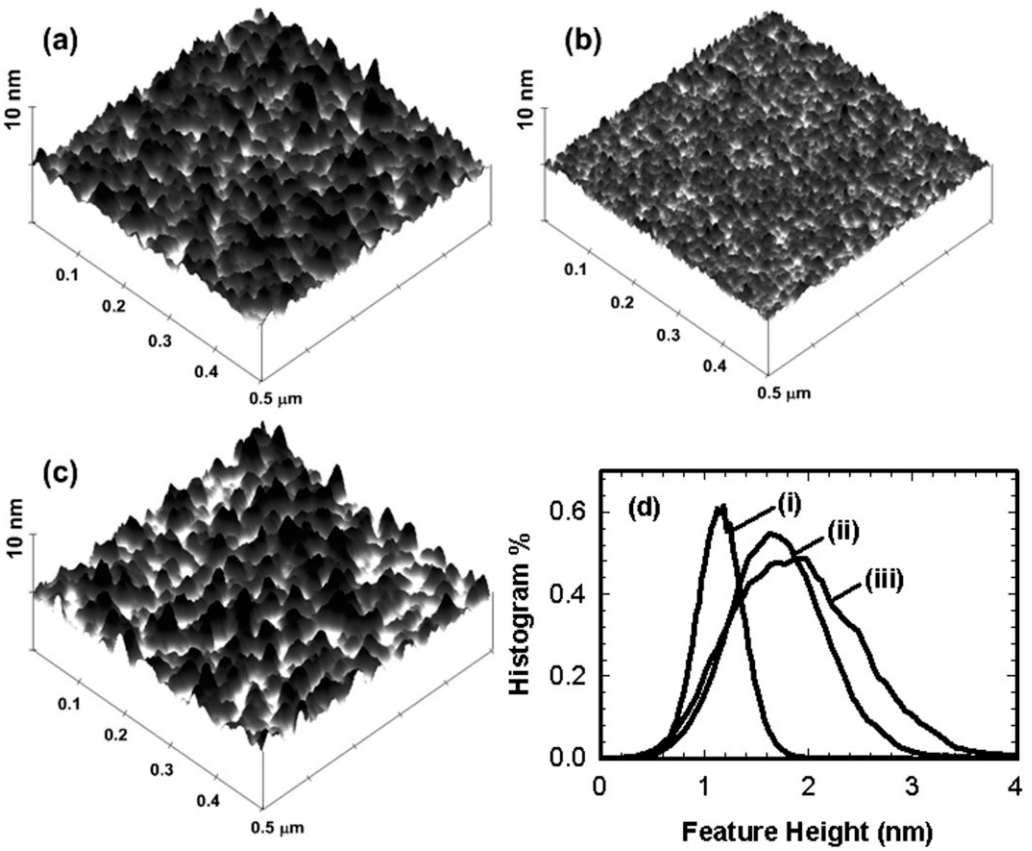

Figure 6 Tapping mode AFM images (0.5×0.5 μm^2) of (a) native silicon, (b) glycidoxy-grafted silicon, and (c) azo-glycidoxy-grafted silicon with the corresponding (d) polymer surface feature height distributions.

grafting to the surface, and therefore, φ_{surf} for controlled polymerization reactions represents only the contribution of monomer addition to the surface. Notwithstanding, the graft fraction for the controlled reaction, at a catalyst to initiator ratio of 2 : 1, was greater than for the uncontrolled reaction (i.e., catalyst to initiator ratio of 0 : 1), with a range of 4.5% to 5.6% relative to 3.6% to 4.8%, respectively. An increase in graft fraction for the controlled reaction was expected, given the higher graft yield which was achieved by reversible capping of the growing surface chains by reverse ATRGP. However, the low graft fraction achieved with both FRGP and reverse ATRGP suggests that the initiation efficiency was greater in solution than at the surface ($f_b >> f_s$), possibly due to hindered monomer diffusion into the polymer surface layer and initiator cage effects which favor solution-phase initiation.[18]

The surface topography of the graft polymerized surface was evaluated by tapping mode Atomic Force Microscopy (AFM) for silicon wafers that were modified by the same reaction conditions as for the silica particles. Comparison of the AFM images of native silicon [Fig. 6(a)], glycidoxy-grafted silicon [Fig. 6(b)], and azo-glycidoxy-grafted silicon [Fig. 6(c)] demonstrated the relatively spatially uniform coverage achieved by self-assembled glycidoxy chemistry on the silicon substrate. The layer thickness, defined as the z-height distance measured by AFM from the highest to lowest elevation on the surface ($\Delta Z_t = Z_{max} - Z_{min}$), RMS surface roughness [R_{RMS}, eq. (17)], skewness [S_{skew}, eq. (18)], and material volume (i.e., layer thickness integrated over the x-y plane) are provided in Table III. The glycidoxy-grafted silicon substrates exhibited a 70% increase in layer thickness, a threefold increase in surface roughness, and a 50% increase in grafted material volume, compared to the native silicon substrate (Table III). Similarly, the azo modified surface had a 40% increase in layer thickness ($Z = 4.33$ nm) and a 33% increase in surface roughness ($R_{RMS} = 0.64$ nm), relative to the glycidoxy-grafted surface (Table III). The feature height profile [Fig. 6(d)] illustrated an increase in the skewness of the height distribution for the glycidoxy-silane ($S_{skew} = 0.22$) and azo initiator layers ($S_{skew} = 0.26$), compared to the native silicon surface ($S_{skew} = 0.01$). However, the increase in the skewness of the distribution would be expected for monolayer self-assembly on a substrate surface. It was interesting to note, though, that only an 18% increase in skewness was observed during the azo conversion of the glycidoxy-silane layer.

TABLE III
Polymer Layer Thickness (nm), Surface Roughness (R_{RMS}), Surface Skewness (S_{skew}), and Material Volume for the Silicon Substrate Modified by Surface Immobilized Initiators and Grafted by FRGP and Reverse ATRGP

Layer	Layer thickness (nm)	R_{RMS} (nm)	S_{skew}	Material volume ($nm^3/\mu m^2$)
Native silicon	1.77	0.16	0.01	1.4×10^5
Glycidoxy-silicon	3.09	0.48	0.22	2.1×10^5
Azo-glycidoxy-silicon	4.33	0.64	0.26	1.0×10^5
FRGP[a]	15.30	1.42	2.85	1.1×10^6
Reverse ATRGP[a]	6.95	1.04	1.08	7.9×10^5

[a] Graft polymerization from azo-glycidoxy-silicon macro initiator surface.

Surface topography, as imaged by AFM, of the P4VP modified substrate prepared by reverse ATRGP (catalyst to initiator molar ratio of 3 : 1) after a 24 h reaction period [Fig. 7(b)] exhibited a more uniform surface feature height distribution, compared to the surface modified by FRGP (catalyst to initiator molar ratio of 0 : 1) [Fig. 7(a)]. The surface roughness of the reverse ATRGP modified surface increased by only 63% ($R_{RMS} = 1.04$ nm), relative to the azo initiator monolayer ($R_{RMS} = 0.64$ nm). In contrast, the surface modified by FRGP exhibited more than a 120% increase in surface roughness ($R_{RMS} = 1.42$ nm), relative to the azo initiator surface. The higher surface roughness for FRGP modified surfaces was the result of a broad feature height profile distribution [Fig. 7(c)], which revealed a distinct tail of high surface features, consistent with the broad molecular weight distribution expected for FRGP. The AFM images revealed the presence of large surface features on the FRGP modified surfaces with feature size (i.e., average diameter) in the range of 60–140 nm [Fig. 7(a)]. In contrast, a more uniform feature height distribution was observed for the reverse ATRGP modified surfaces [Fig. 7(c)], for which a 60% decrease in skewness ($S_{skew} = 1.08$) of the feature height profile was observed, presumably

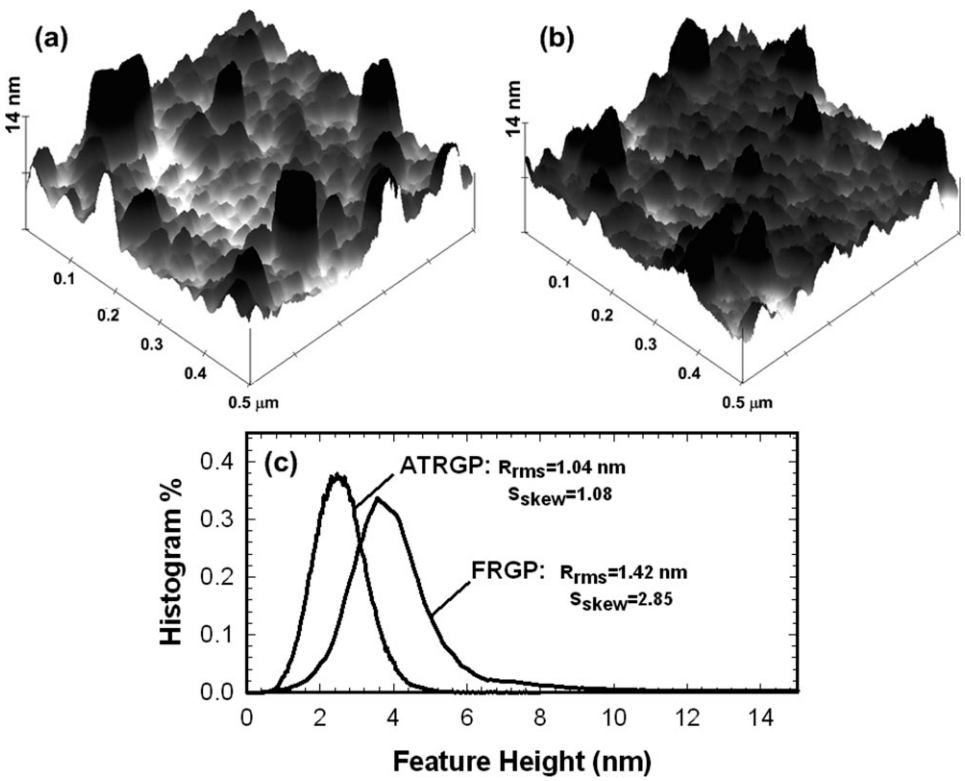

Figure 7 Tapping mode AFM images (0.5×0.5 μm^2) of poly(4-vinylpyridine) modified silicon surfaces by (a) free radical graft polymerization and (b) reverse atom transfer radical graft polymerization with the corresponding height histograms of surface elevations. $[M]_0 = 2.32M$, $[I_2]_0 = 13.6$ mM, $T = 90°C$, and catalyst to initiator ratio of 0 : 1 and 3 : 1 for FRGP and reverse ATRGP, respectively.

due to the presence of smaller surface feature sizes (i.e., average diameter) in the range of 20–45 nm [Fig. 7(b)]. The lower surface roughness and increased uniformity in surface feature height, linear increase in the number-average degree of polymerization with monomer conversion, and lower polydispersity attained in the present reverse ATRGP approach confirm that controlled graft polymerization of 4VP was successfully achieved.

SUMMARY

Controlled radical graft polymerization of 4-vinylpyridine (4VP) onto silica and silicon was demonstrated via reverse atom transfer radical graft polymerization (ATRGP) in an aqueous solvent composed of a 50 vol % mixture of 1-methyl-2-pyrrolidone using azo active site initiators and a $CuCl_2$/2,2′-bipyridine catalyst-ligand complex. Azo surface initiators were immobilized on the silica by conversion of surface-immobilized glycidoxytrimethoxy silane to azobis silane by a reaction with 4,4′-azobis(4-cyanovaleric acid). Controlled reverse ATRGP was demonstrated by first order kinetics with respect to monomer concentration and degree of polymerization that progressed linearly with conversion to yield a $\overline{DP}$ of 115 and 110 for a catalyst to initiator molar ratio of 2 : 1 and 3 : 1, respectively, after a 24 h reaction period. The lowest polydispersity index (PDI) values of 1.30 and 1.28 were also achieved at 2 : 1 and 3 : 1 catalyst to initiator molar ratios, respectively. The polymer graft yield exhibited a linear increase with respect to time for controlled radical polymerization, reaching a graft yield of 8 mg/m^2, a polymer graft density of 0.69 μmol/m^2 (polymer chain spacing of 15.5 Å) and a molecular weight exceeding 12,000 g/mol for a 3 : 1 catalyst to initiator molar ratio. AFM surface analysis confirmed that a more uniform surface feature height distribution was achieved by controlled reverse ATRGP, as demonstrated by a lower RMS surface roughness (R_{RMS} = 1.04 nm) and skewness (S_{skew} = 1.08) of the height profile, relative to the grafted polymer surface prepared by FRGP (R_{RMS} = 1.42 nm; S_{skew} = 2.85).

This work was funded in part, by the USEPA, the California Department of Water Resources, and the USDOE.

References

1. Rovira-Bru, M.; Giralt, F.; Cohen, Y. J Colloid Interface Sci 2001, 235, 70.
2. Cohen, Y.; Eisenberg, P.; Chaimberg, M. J Colloid Interface Sci 1992, 148, 579.
3. Krasilnikov, I.; Borisova, V. J Chromatogr 1988, 446, 211.
4. Papirer, E.; Nguyen, V. T.; Morawski, J. C.; Donnet, J. B. Eur Polym J 1975, 11, 597.
5. Voronov, A.; Kohut, A.; Synytska, A.; Peukert, W. J Appl Polym Sci 2007, 104, 3708.
6. Yokoyama, R.; Suzuki, S.; Shirai, K.; Yamauchi, T.; Tsubokawa, N.; Tsuchimochi, M. Eur Polym J 2006, 42, 3221.
7. Laible, R.; Hamann, K. Adv Colloid Interface Sci 1980, 13, 65.
8. Jou, J. D.; Yoshida, W.; Cohen, Y. J Membr Sci 1999, 162, 269.
9. Yamaguchi, T.; Miyazaki, Y.; Nakao, S.; Tsuru, T.; Kimura, S. Ind Eng Chem Res 1998, 37, 177.
10. Castro, R. P.; Cohen, Y.; Monbouquette, H. G. J Membr Sci 1996, 115, 179.
11. Yamaguchi, T.; Yamahara, S.; Nakao, S.; Kimura, S. J. J Membr Sci 1994, 95, 39.
12. Castro, R. P.; Cohen, Y.; Monbouquette, H. G. J Membr Sci 1993, 84, 151.
13. Jayakumar, R.; Prabaharan, M.; Reis, R. L.; Mano, J. F. Carbohydr Polym 2005, 62, 142.
14. Morinaga, H.; Ochiai, B.; Mori, H.; Endo, T. J Polym Sci Part A: Polym Chem 2006, 44, 3778.
15. Tsubokawa, N.; Kuroda, A.; Sone, Y. J Polym Sci Part A: Polym Chem 1989, 27, 1701.
16. Tsubokawa, N.; Kogure, A.; Maruyama, K.; Sone, Y.; Shimomura, M. Polym J 1990, 22, 827.
17. Prucker, O.; Ruhe, J. Macromolecules 1998, 31, 602.
18. Nguyen, V.; Yoshida, W.; Jou, J. D.; Cohen, Y. J Polym Sci Part A: Polym Chem 2002, 40, 26.
19. Nguyen, V.; Yoshida, W.; Cohen, Y. J Appl Polym Sci 2003, 87, 300.
20. Xia, J. H.; Matyjaszewski, K. Macromolecules 1997, 30, 7692.
21. Matyjaszewski, K.; Patten, T. E.; Xia, J. H. J Am Chem Soc 1997, 119, 674.
22. Matyjaszewski, K. Macromolecules 1998, 31, 4710.
23. Matyjaszewski, K.; Xia, J. H. Chem Rev 2001, 101, 2921.
24. Davis, K. A.; Paik, H. J.; Matyjaszewski, K. Macromolecules 1999, 32, 1767.
25. Wang, J. L.; Grimaud, T.; Matyjaszewski, K. Macromolecules 1997, 30, 6507.
26. Ejaz, M.; Yamamoto, S.; Ohno, K.; Tsujii, Y.; Fukuda, T. Macromolecules 1998, 31, 5934.
27. Percec, V.; Barboiu, B.; Kim, H. J. J Am Chem Soc 1998, 120, 305.
28. Perruchot, C.; Khan, M. A.; Kamitsi, A.; Armes, S. P.; von Werne, T.; Patten, T. E. Langmuir 2001, 17, 4479.
29. Zhang, H. Q.; Klumperman, B.; Ming, W. H.; Fischer, H.; van der Linde, R. Macromolecules 2001, 34, 6169.
30. Gromada, J.; Matyjaszewski, K. Macromolecules 2001, 34, 7664.
31. Xia, J. H.; Zhang, X.; Matyjaszewski, K. Macromolecules 1999, 32, 3531.
32. Matyjaszewski, K.; Davis, K.; Patten, T. E.; Wei, M. L. Tetrahedron 1997, 53, 15321.
33. Coessens, V.; Matyjaszewski, K. J Macromol Sci Pure Appl Chem 1999, 36, 811.
34. Shah, R. R.; Merreceyes, D.; Husemann, M.; Rees, I.; Abbott, N. L.; Hawker, C. J.; Hedrick, J. L. Macromolecules 2000, 33, 597.
35. Huang, X. Y.; Doneski, L. J.; Wirth, M. J. Chem Tech 1998, 28, 19.
36. Huang, X. Y.; Doneski, L. J.; Wirth, M. J. Anal Chem 1998, 70, 4023.
37. Huang, X. Y.; Wirth, M. J. Anal Chem 1997, 69, 4577.
38. Tsujii, Y.; Ejaz, M.; Yamamoto, S.; Fukuda, T.; Shigeto, K.; Mibu, K.; Shinjo, T. Polymer 2002, 43, 3837.
39. Gopireddy, D.; Husson, S. M. Macromolecules 2002, 35, 4218.
40. Min, K.; Hu, J. H.; Wang, C. C.; Elaissari, A. J Polym Sci Part A: Polym Chem 2002, 40, 892.
41. Jayach andran, K. N.; Takacs-Cox, A.; Brooks, D. E. Macromolecules 2002, 35, 6070.
42. Carlmark, A.; Malmstrom, E. J Am Chem Soc 2002, 124, 900.
43. Kusumo, A.; Bombalski, L.; Lin, Q.; Matyjaszewski, K.; Schneider, J. W.; Tilton, R. D. Langmuir 2007, 23, 4448.

44. Lokuge, I.; Wang, X.; Bohn, P. W. Langmuir 2007, 23, 305.
45. Mu, B.; Wang, T. M.; Liu, P. Ind Eng Chem Res 2007, 46, 3069.
46. Fu, G. D.; Zhao, J. P.; Sun, Y. M.; Kang, E. T.; Neoh, K. G. Macromolecules 2007, 40, 2271.
47. Save, M.; Granvorka, G.; Bernard, J.; Charleux, B.; Boissiere, C.; Grosso, D.; Sanchez, C. Macromol Rapid Commun 2006, 27, 393.
48. Sanjuan, S.; Perrin, P.; Pantoustier, N.; Tran, Y. Langmuir 2007, 23, 5769.
49. Matyjaszewski, K.; Dong, H. C.; Jakubowski, W.; Pietrasik, J.; Kusumo, A. Langmuir 2007, 23, 4528.
50. Ayres, N.; Boyes, S. G.; Brittain, W. J. Langmuir 2007, 23, 182.
51. Wang, Y.; Hu, S. W.; Brittain, W. J. Macromolecules 2006, 39, 5675.
52. Zhang, M. M.; Liu, L.; Zhao, H. Y.; Yang, Y.; Fu, G. Q.; He, B. L. J Colloid Interface Sci 2006, 301, 85.
53. Goodman, D.; Kizhakkedathu, J. N.; Brooks, D. E. Langmuir 2004, 20, 2333.
54. Liu, D. M.; Chen, Y. W.; Zhang, N.; He, X. H. J Appl Polym Sci 2006, 101, 3704.
55. Couet, J.; Biesalski, M. Macromolecules 2006, 39, 7258.
56. Xu, Y. Q.; Xu, Q. F.; Lu, J. M.; Xia, X. W.; Wang, L. H. Polym Bull 2007, 58, 809.
57. Moineau, G.; Dubois, P.; Jerome, R.; Senninger, T.; Teyssie, P. Macromolecules 1998, 31, 545.
58. Braunecker, W. A.; Matyjaszewski, K. J Mol Catal A: Chem 2006, 254, 155.
59. Baggiani, C.; Giraudi, G.; Giovannoli, C.; Tozzi, C.; Anfossi, L. Anal Chim Acta 2004, 504, 43.
60. Navarro-Villoslada, F.; San Vicente, B.; Moreno-Bondi, M. C. Anal Chim Acta 2004, 504, 149.
61. Luz, C. T. L.; Coutinho, F. M. B. Eur Polym J 2000, 36, 547.
62. Coutinho, F. M. B.; Carvalho, D. L.; Aponte, M. L. L.; Barbosa, C. C. R. Polymer 2001, 42, 43.
63. Neagu, V.; Untea, I.; Tudorache, E.; Luca, C. React Funct Polym 2003, 57, 119.
64. Malik, M. A.; Mukhtar, R.; Zaidi, S. A. R.; Ahmed, S.; Awan, M. A. React Funct Polym 2002, 51, 117.
65. Ying, L.; Zhai, G.; Winata, A. Y.; Kang, E. T.; Neoh, K. G. J Colloid Interface Sci 2003, 265, 396.
66. Zhai, G. Q.; Kang, E. T.; Neoh, K. G. J Membr Sci 2003, 217, 243.
67. Lewis, G. T.; Nguyen, V.; Cohen, Y. J Polym Sci Part A: Polym Chem 2007, 45, 5748.
68. Wei, X. L.; Li, X.; Husson, S. M. Biomacromolecules 2005, 6, 1113.
69. Ayres, N.; Cyrus, C. D.; Brittain, W. J. Langmuir 2007, 23, 3744.
70. Yu, K.; Wang, H. F.; Xue, L. J.; Han, Y. C. Langmuir 2007, 23, 1443.
71. Singh, N.; Husson, S. M.; Zdyrko, B.; Luzinov, I. J Membr Sci 2005, 262, 81.
72. Cheng, Z. P.; Zhu, X. L.; Shi, Z. L.; Neoh, K. G.; Kang, E. T. Surf Rev Lett 2006, 13, 313.
73. Li, D. X.; He, Q.; Cui, Y.; Li, J. B. Chem Mater 2007, 19, 412.
74. Chaimberg, M.; Cohen, Y. AIChE J 1994, 40, 294.
75. Pere, E.; Cardy, H.; Cairon, O.; Simon, M.; Lacombe, S. Vib Spectrosc 2001, 25, 163.
76. Yoshida, W.; Castro, R. P.; Jou, J. D.; Cohen, Y. Langmuir 2001, 17, 5882.
77. Tsubokawa, N.; Shirai, Y.; Tsuchida, H.; Handa, S. J Polym Sci Part A: Polym Chem 1994, 32, 2327.